AIAA JOURNAL
Vol. 43, No. 4, April 2005

Surface Modification Method for Aerodynamic Design Optimization

Hyoung-Jin Kim,* Salim Koc,† and Kazuhiro Nakahashi‡
Tohoku University, Sendai 980-8579, Japan

A new geometry modification method for aerodynamic design optimization is developed using surface mesh coordinates as design variables. Surface meshes are modeled as a spring system with tension and bending springs, and a negative gradient vector of a design objective function is imposed on the spring system as fictitious external forces. Corresponding deformation of the surface spring system is considered as a smoothed vector of the objective function gradient and used for a line search to find an optimum solution along the smoothed vector. This provides a rich design space, which is limited only by the surface mesh density. It also enables smooth variation of design surfaces even for singular gradient vectors. As design examples, sample aerodynamic optimization problems are conducted utilizing two- and three-dimensional computational-fluid-dynamics codes for flow analyses and discrete adjoint codes for sensitivity analyses. A recommendation on the selection of a required parametric value is made based on the design results.

Nomenclature

F	=	objective function for design optimization
k	=	spring stiffness coefficient
N_{edge}	=	number of surface edges connected to a node ($= N_{\text{neib}}$)
N_{neib}	=	number of neighboring surface nodes for a node
N_{node}	=	total number of nodes on the design surface
T	=	fictitious load imposed on node
α	=	incidence angle
Δx	=	displacement of mesh point coordinates

Subscripts

b	=	bending
e	=	external force
t	=	tension

Superscript

*	=	target value

I. Introduction

WITH the advances in computational fluid dynamics (CFD) and computing power of modern computers, aerodynamic design optimization methods utilizing CFD techniques are more important than ever. Among several design optimization methods applicable to aerodynamic design problems, gradient-based methods have been used most widely because of their well-developed numerical algorithms and relatively small computational burden.

In the application of gradient-based methods to practical aerodynamic design problems, one of the major concerns is accurate and efficient calculation of sensitivity gradients of aerodynamic objective functions. During the last decade, the adjoint method has gained much attention as an efficient method of sensitivity analysis for aerodynamic optimization because it allows calculation of sensitivity information independent of the number of design variables.[1–9]

For practical aerodynamic design optimization of complex three-dimensional configurations, an efficient and robust geometry modification method is also required. There are several geometry parameterization approaches for shape optimization including the mesh-point method, the shape function method, the spline method, the free-form deformation method, and so on. Readers are referred to Ref. 10 for a survey of geometric parameterization methods for shape optimization applications.

Among the several geometric modification methods, the mesh-point approach directly uses surface grid-point coordinates as design variables. It provides a rich design space, possible geometric variation being limited only by the density of the surface mesh points. If all of the surface node points are allowed to move, the number of design variables can easily reach tens of thousands in three-dimensional design problems for entire aircraft. For such a large number of design variables, use of an adjoint method is essential to obtain sensitivity information efficiently. Also, the large number of design variables prevents the use of high-order optimization algorithms such as the quasi-Newton method because of memory limitations.[6]

A drawback of the mesh-point approach is that it is hard to obtain a smooth geometry variation. This is because an objective function gradient with respect to surface mesh coordinates in aerodynamic optimization is not smooth and often contains high-frequency oscillations, and the geometric variation is proportional to the objective function gradient. To keep the design surface smooth in the mesh-point approach, smoothing methods need to be incorporated.

The most widely employed method for smoothing in the mesh-point approach is the Sobolev implicit smoothing method,[1,9] which is used for smoothing of an objective function gradient[1] or geometric variation.[9] In addition to its smoothing effect, Sobolev implicit smoothing also acts as a preconditioner that allows use of much larger steps for a line search procedure of gradient-based optimization and leads to a large reduction in the number of design iterations needed for convergence.[1] However, Sobolev implicit smoothing has been found to be unable to eliminate fluctuations in the gradient in problems with oscillating gradient vectors.[11]

Another method that can be employed for smoothing in the mesh-point approach is the traction method, which was suggested by Azegami[12,13] and Katamine and Azegami[14] for shape optimization in elliptic boundary-value problems. In the traction method, a set of fictitious forces, which is a negative gradient of an objective function, is imposed on the surface mesh points as external forces causing a geometric deformation. The geometric deformation is the displacement of an analogy elastic problem, which is obtained by finite

Received 1 June 2004; presented as Paper 2004-2328 at the AIAA 34th Fluid Dynamics Conference, Portland, OR, 28 June–1 July 2004; revision received 6 October 2004; accepted for publication 12 October 2004.

*Research Associate, Department of Aeronautics and Space Engineering. Member AIAA.

†Graduate Student, Department of Aeronautics and Space Engineering. Student Member AIAA.

‡Professor, Department of Aeronautics and Space Engineering. Associate Fellow AIAA.

element analysis. This method has been applied mainly to structural optimization of elastic bodies and extended to vibration and potential flow problems.[13,14] Because a surface mesh point with a large objective gradient would experience large deformation and because such deformation must be smooth for analogy elastic problems, the concept of the traction method is quite reasonable for smoothing the geometric variation with an oscillating gradient vector.

On the other hand, the natural design approach[15] directly uses fictitious loads on surface grid points as design variables instead of node point coordinates. The displacements produced by the fictitious forces are added to the initial grid points to obtain a new shape. Consequently, the relationship between the changes in design variables and grid-point displacement is established through finite element analysis. In Ref. 15, this approach was applied to a structural optimum shape design of an elastic body. This approach also guarantees a smooth design surface. However, because the required number of finite element analyses for objective gradient calculation is the same as the number of design variables (i.e., fictitious loads), the required computational cost would become prohibitively great for design problems with a large number of design variables. This is in contrast to the traction method, in which finite element analysis for surface deformation is required only once per one design iteration.

In this study, a new surface modification method using coordinates of surface mesh points as design variables is developed for aerodynamic optimization. For a smooth variation of the surface geometry, we employ the concept of the traction method. To reduce computational cost of the original traction method, the spring analogy is adopted instead of finite element analysis for the design surface. The objective function gradient is efficiently calculated by an adjoint method. A negative gradient of the objective function is imposed on the surface nodes as nodal forces. The resultant deformation of the geometry is used as a smoothed direction vector for the design, and a line search is conducted along the direction vector. The overall procedure is repeated until convergence.

In this paper, the validity of the present method is demonstrated for two-dimensional viscous and three-dimensional inviscid design examples. For the flow and sensitivity analysis of two-dimensional examples, a structured grid Reynolds-averaged Navier–Stokes solver and its discrete adjoint code are utilized. For three-dimensional cases, an unstructured grid Euler solver and its discrete adjoint code are used.

The paper is organized as follows. In Sec. II, detailed formulation of the present surface modification method is described for two- and three-dimensional cases. A brief description on the flow solvers and adjoint codes is given in Sec. III, which is followed by presentation of design strategy, including the optimization algorithm and the method of volume grid modification, in Sec. IV. Design results utilizing the present design method are then given in Sec. V for inverse and direct design of transonic airfoils as two-dimensional examples and transonic wing and supersonic fuselage designs as three-dimensional examples. Finally, conclusions are presented in Sec. VI.

II. Traction Method and Spring Analogy

A. Traction Method: The Original Approach[12–14]

When using all of the surface mesh points as design variables, smoothness of the resulting design surface is not guaranteed if the design surface is modified proportional to an objective function gradient. This is because of fluctuations in the objective function gradient.

The traction method was developed to cope with the smoothness problem when using all of the surface mesh points as design variables. In the traction method, the geometry under design is considered as an elastic body. Instead of the geometric variations proportional to the objective function gradient on the surface mesh points, a set of fictitious forces, which is a negative gradient of the objective function, is imposed on the surface mesh points as external forces causing a geometric deformation of the elastic body. A one-dimensional search is conducted along the deformation vector.

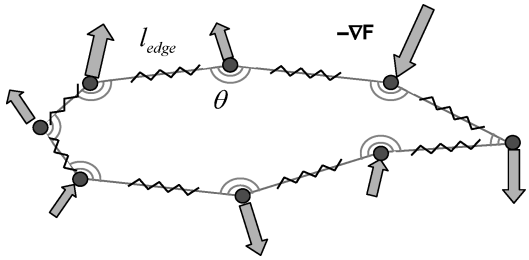

Fig. 1 Schematic diagram of traction method with spring analogy.

In the original traction method, the geometric deformation by the fictitious forces is calculated by finite element analysis for the pseudoelastic boundary-value problem. The traction method guarantees smoothness of the design surface deformation. It was also proved that the domain deformation by the external forces reduces the objective function if the one-dimensional marching step along the deformation vector is sufficiently small.

B. Traction Method: The Present Approach in Two Dimensions

In the present study, we employ the concept of the traction method for aerodynamic design optimization using all of the surface mesh points as design variables. However, instead of the finite element method for the pseudoelastic body model a spring-analogy approach is adopted for the design surface mesh points for more efficient calculation of geometric variation as a result of the fictitious forces.

Spring analogy has been widely used for volume grid modification of dynamic grids for flow analysis around a moving body because of its simplicity and efficiency.[16,17] In the present approach, the geometric surface is modeled as a spring system, in which edges are regarded as tension springs and node points as bending springs. A schematic diagram of this concept is depicted in Fig. 1 for a two-dimensional airfoil. Tension spring forces work to reduce slopes in geometric variations, while bending spring forces act to reduce curvatures of the geometry variation, which makes the deformation smooth.

The elastic energy of tension and bending springs can be expressed for two-dimensional cases as follows:

$$E_t = \frac{1}{2}\sum_{i=1}^{N_{\text{node}}-1} k_t(\Delta x_{i+1} - \Delta x_i)^2 \tag{1}$$

$$E_b = \frac{1}{2}\sum_{i=1}^{N_{\text{node}}} k_b(\Delta x_{i-1} - 2\Delta x_i + \Delta x_{i+1})^2 \tag{2}$$

The tension and bending spring coefficients are defined as follows:

$$k_t = 1/l_{\text{edge}} \tag{3a}$$

$$k_b = C_b \sin\theta \tag{3b}$$

where l_{edge} is edge length, θ is variation of the angle between two edges sharing a node, and C_b is a parametric bending constant to control the balance between the bending spring force and tension spring force. The potential energy by the external force T is written as

$$E_e = -\sum_{i=1}^{N_{\text{node}}} T_{xi}\Delta x_i \tag{4}$$

Total elastic potential energy of the spring system is $E = E_t + E_b + E_e$. For the deformation of equilibrium state, partial derivatives of the potential energy with respect to a geometric variation diminish:

$$\frac{\partial E}{\partial \Delta x} = \frac{\partial E_t}{\partial \Delta x} + \frac{\partial E_b}{\partial \Delta x} + \frac{\partial E_e}{\partial \Delta x} = 0 \tag{5}$$

which results in a system of equations as follows:

$$k_{b_{i-1}}\Delta x_{i-2} - \left(2k_{b_{i-1}} + 2k_{b_i} + k_{t_{i-1}}\right)\Delta x_{i-1} + \left(k_{b_{i-1}} + 4k_{b_i} + k_{b_{i+1}} + k_{t_{i-1}} + k_{t_i}\right)\Delta x_i - \left(2k_{b_i} + 2k_{b_{i+1}} + k_{t_i}\right)\Delta x_{i+1} + k_{b_{i+1}}\Delta x_{i+2} = T_i \tag{6}$$

The preceding equations can be represented in a matrix form as follows:

$$[K]\{\Delta X\} = \{T\} \tag{7}$$

which can be solved by Jacobi iteration or other iterative methods. Computional cost for the solution of Eq. (7) is negligible compared to the cost of flow and adjoint analyses.

C. Sobolev Implicit Smoothing

Sobolev implicit smoothing has been widely used for the smoothing of the objective function gradient vector.[1,9] For purposes of comparison, the Sobolev implicit smoothing is also implemented here for a two-dimensional case. The equation for the Sobolev implicit smoothing is given as follows[1]:

$$(I - \varepsilon\nabla^2)\boldsymbol{\delta\bar{x}} = \boldsymbol{\delta x} \tag{8}$$

where $\boldsymbol{\delta x}$ is the initial vector before smoothing, $\boldsymbol{\delta\bar{x}}$ is the smoothed vector, and ε is a smoothing factor. A larger ε gives a smoother profile of the vector components. For a two-dimensional case with one-dimensional surface nodes, Eq. (8) becomes

$$\boldsymbol{\delta\bar{x}}_i - \varepsilon(\boldsymbol{\delta\bar{x}}_{i+1} - 2\boldsymbol{\delta\bar{x}}_i + \boldsymbol{\delta\bar{x}}_{i-1}) = \boldsymbol{\delta x}_i \tag{9}$$

To compare the smoothing performance of the present traction method and the Sobolev implicit smoothing method, a singular force $T = 0.1$ is imposed on an airfoil surface node point. As can be seen in Fig. 2, the traction method results in a smooth deformation (or a smoothed vector) for a sufficiently large bending constant. On the other hand, the Sobolev implicit method gives a peaky shape variation even for very large smoothing factors. Although the smoothing factor ε presented in the Fig. 2 is up to 100, larger values also give similar peaky shapes with much lower magnitude. Instead of a constant value for ε throughout the domain, we tested other definitions of ε such as the second derivatives of $\boldsymbol{\delta\bar{x}}$, which were also found to result in peaky distributions.

Figure 3 shows additional results of the present traction method by upward and downward singular force imposition on the upper surface of an airfoil. The traction method gives a smooth deformation for singular external forces.

D. Traction Method: The Present Approach in Three Dimensions

The present concept, in which the traction method is adopted, can be extended to three-dimensional surface meshes. The elastic energy of tension and the bending springs for three-dimensional surface mesh deformation can be represented by

$$E_t = \frac{1}{2}\sum_{i=1}^{N_{\text{edge}}} k_{t_i}(\Delta x_{i+1} - \Delta x_i)^2 \tag{10}$$

$$E_b = \frac{1}{2}\sum_{i=1}^{N_{\text{node}}} \frac{k_{b_i}}{N_{\text{neib}}}\left(\sum_{j=1}^{N_{\text{neib}}} \Delta x_j N_{\text{neib}} - \Delta x_i\right)^2 \tag{11}$$

The bending stiffness coefficient k_b at a node is defined in Eq. (12) as an average of $\sin\theta$ of neighboring nodes, where θ is an angle between the initial and deformed edges as shown in Fig. 4:

$$k_{b_i} = \frac{C_b}{N_{\text{neib}}}\sum_{j=1}^{N_{\text{neib}}} \sin\theta_j \tag{12}$$

The definition of k_t is the same as in the two-dimensional case in Eq. (3a).

The potential energy by the external force T, the negative gradient of the objective function, is defined as follows:

$$E_e = -\sum_{i=1}^{N_{\text{node}}} T_i \Delta x_i \tag{13}$$

Total elastic potential energy of the spring system is $E = E_t + E_b + E_e$ as in the two-dimensional case. A system of equations can also be obtained by taking the derivative of the total potential energy with respect to geometric variation Δx at a node point n to be zero as in the two-dimensional case in Eq. (5). Each term of the potential energy derivative becomes

$$\frac{\partial E_t}{\partial \Delta x_n} = \sum_{i=1}^{N_{\text{edge}}} k_{t_i}(\Delta x_n - \Delta x_i) \tag{14}$$

$$\frac{\partial E_b}{\partial \Delta x_n} = -k_{b_n} N_{\text{neib}}\left(\sum_{i=1}^{N_{\text{neib}}} \Delta x_i - \Delta x_n N_{\text{neib}}\right) + \sum_{i=1}^{N_{\text{neib}}} k_{b_i}\left(\sum_{j=1}^{N_{\text{neib}_i}} \Delta x_j - \Delta x_i N_{\text{neib}_i}\right) \tag{15}$$

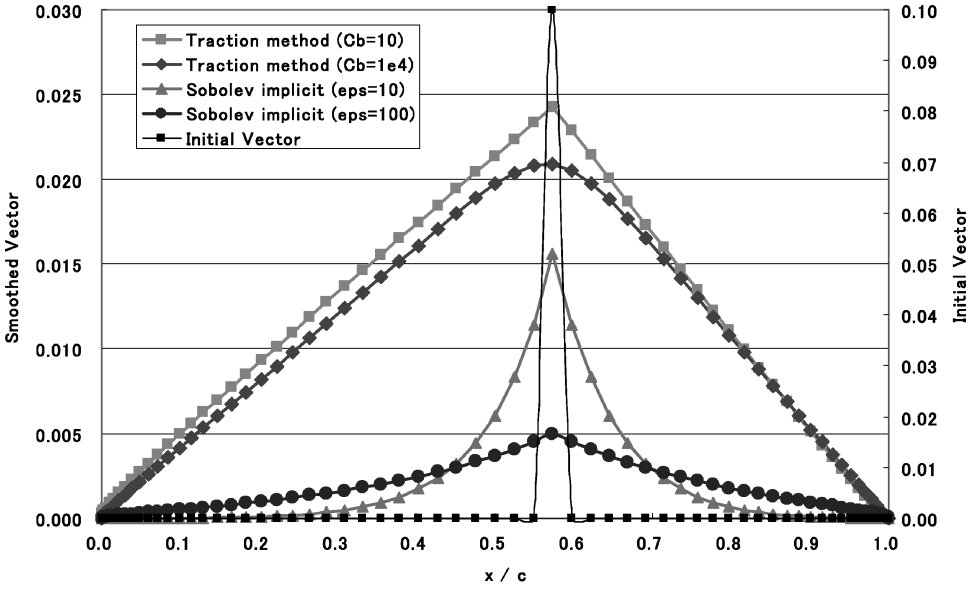

Fig. 2 Comparison of traction method and Sobolev implicit smoothing for a singular force on airfoil surface.

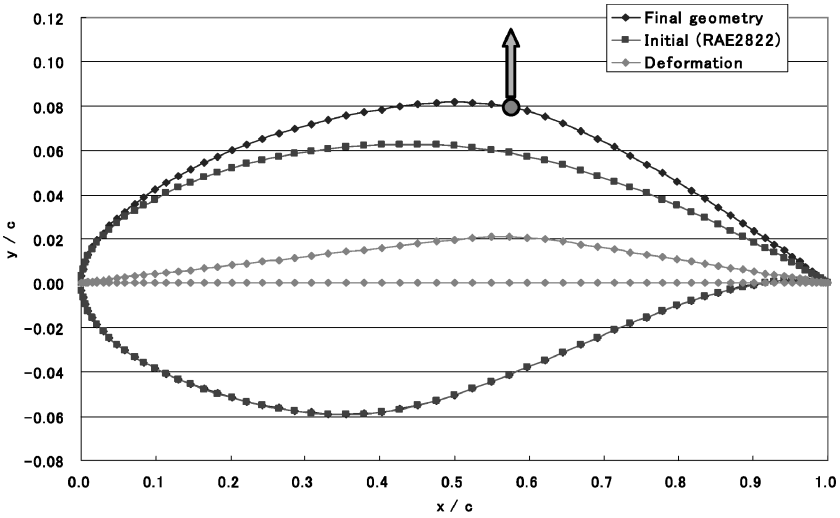

a) Upward fictitious force

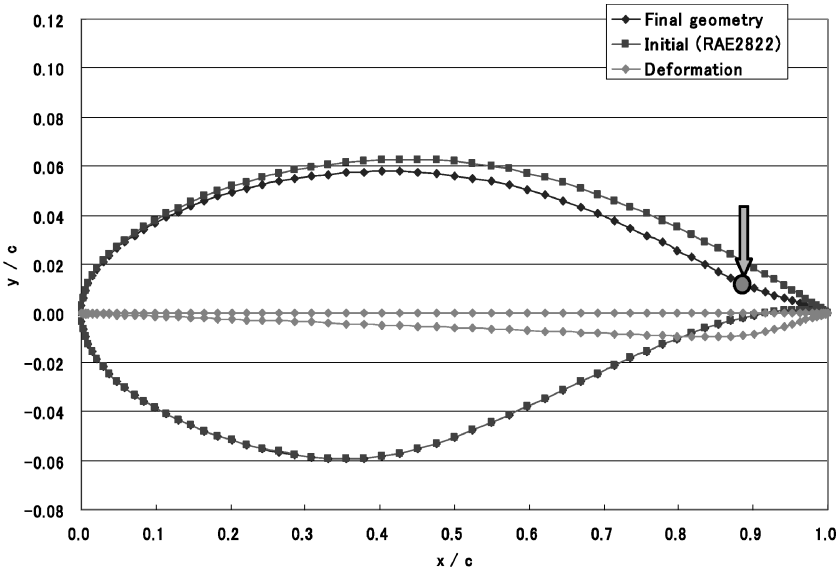

b) Downward fictitious force

Fig. 3 Deformation by singular forces on airfoil surface using traction method.

$$\frac{\partial E_e}{\partial \Delta x_n} = -T_n \tag{16}$$

where index i represents neighboring nodes of node n, and index j is the neighboring nodes of node i. Note that node n is one of the neighboring nodes of node j.

If we sum Eqs. (14–16) and arrange them with N_{edge} being equal to N_{neib}, the following equation is obtained:

$$\left(\sum_{i=1}^{N_{\text{neib}_n}} k_{t_i} + k_{b_n} N_{\text{neib}_n}^2 + \sum_{i=1}^{N_{\text{neib}_n}} k_{b_i}\right)\Delta x_n = \sum_{i=1}^{N_{\text{neib}_n}} \left[\left(k_{t_i} + k_{b_n} N_{\text{neib}_n} + k_{b_i} N_{\text{neib}_i}\right)\Delta x_i - k_{b_i} \sum_{\substack{j=1 \\ j\neq n}}^{N_{\text{neib}_i}} \Delta x_j\right] + T_n \tag{17}$$

Solution of this system of equations can be obtained by using the Jacobi iteration method or other iterative methods. The computational cost for the solution of Eq. (17) is negligible compared to the cost of flow and adjoint analyses. The two-dimensional formulation derived in Sec. II.B can be considered as a special case of the preceding three-dimensional formulations in which a surface node point has only two neighboring nodes.

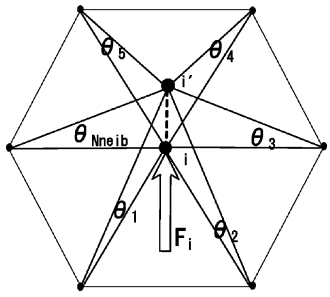

Fig. 4 Definition of θ for bending stiffness on three-dimensional surface mesh.

III. Flow and Sensitivity Analysis

A. Two-Dimensional Flow Analysis

For two-dimensional design examples, a structured grid Navier–Stokes solver[18,19] is used for the flow analysis. Two-dimensional Reynolds-averaged compressible Navier–Stokes equations in generalized coordinates are used in the conservation form based on the finite volume cell-centered approach. Roe's flux-difference-splitting (FDS) scheme[20] was adopted for the space discretization of the inviscid flux terms. A monotone upstream centered scheme for conservation law (MUSCL) approach[21] is used with a limiter to obtain a third order of spatial accuracy. Second-order central differencing

is used for the viscous flux terms of the residual vector. Beam and Warming's alternating-direction-implicit (ADI) method is used for the time integration, and local time stepping is used. Turbulence effects are considered using the Baldwin–Lomax algebraic model with a relaxation technique.[22] The computational grid is a C-type one with 169×61 total grid points and 129 points on the airfoil surface. Details of the flow solver can be found in Ref. 18.

B. Three-Dimensional Flow Analysis

For three-dimensional design examples, an unstructured mesh Euler solver is used as a flow solver. The governing Euler equations are solved by the finite volume cell-vertex scheme. Control volumes are nonoverlapping dual cells constructed around each node. Each edge connecting two nodes is associated with an area vector of the control surface, and gas dynamic fluxes are computed through the areas. To enhance the accuracy of the scheme, a linear reconstruction of the primitive gas dynamic variables inside the control volume is used combined with Venkatakrishnan's limiter.[23] The flux is computed using the Harten-Lax-van Leer-Einfeldt-Wada (HLLEW) approximate Riemann solver.[24] For the time integration, the lower-upper symmetric Gauss–Seidel (LU-SGS) implicit method is adopted.[25] Details of the flow solver can be found in Ref. 25.

C. Sensitivity Analysis: Discrete Adjoint Method

In this section, we briefly discuss on the discrete adjoint codes for sensitivity analysis. Details of the adjoint codes can be found in Refs. 7 and 8.

The discrete adjoint equation is given as follows:

$$\frac{\partial \boldsymbol{R}^T}{\partial \boldsymbol{Q}}\boldsymbol{\Lambda} + \frac{\partial F}{\partial \boldsymbol{Q}} = 0 \tag{18}$$

where $\boldsymbol{R}$ is the residual vector of a flow solver, $\boldsymbol{Q}$ is the flow variable vector, and F is an aerodynamic objective function. If the preceding adjoint equation is solved for the adjoint variable vector $\boldsymbol{\Lambda}$, the sensitivity gradient of F can be efficiently calculated by the following equation without any information on the flow variable sensitivity $\partial \boldsymbol{Q}/\partial\beta$:

$$\frac{\mathrm{d}F}{\mathrm{d}\beta} = \frac{\partial F^T}{\partial \boldsymbol{X}}\frac{\mathrm{d}\boldsymbol{X}}{\mathrm{d}\beta} + \frac{\partial F}{\partial \beta} + \boldsymbol{\Lambda}^T\left(\frac{\partial \boldsymbol{R}}{\partial \boldsymbol{X}}\frac{\mathrm{d}\boldsymbol{X}}{\mathrm{d}\beta} + \frac{\partial \boldsymbol{R}}{\partial \beta}\right) \tag{19}$$

where $\boldsymbol{X}$ is the grid position vector and $d\boldsymbol{X}/d\beta$ is the grid sensitivity, which can be calculated by a finite difference approximation or by direct differentiation of a routine for the grid generation or modification.

Both of the adjoint codes utilized in the present study are developed by manually differentiating the residual calculation routines of the flow solvers. The adjoint codes are differentiated in a full discrete manner, in which the reconstructions and approximate Riemann solvers in the flow solvers are exactly differentiated. The viscous flux terms of the two-dimensional Navier–Stokes solver are also exactly differentiated. A pseudotime term is added to the adjoint equation of Eq. (18), which is then solved by the same time integration scheme with the flow solvers.[7,8,26]

Because the smoothed gradient is used in the design process instead of the actual exact gradient, the adjoint code does not need to be fully converged to calculate very accurate sensitivity derivatives. In the present study, a convergence criterion of one order reduction from an initial residual in adjoint analysis was found enough for successful design convergences. This allows reduction of computational cost for sensitivity analysis by more than half compared with cases using nonsmoothed exact gradient information in which more than two orders of adjoint residual reduction is usually required for adjoint analyses.[3,7]

IV. Design Strategy

A. Design Variables

In the traction method, design variables can be defined as either x, y, z coordinates or normal, tangential coordinates of surface meshes. Instead of using all of the surface meshes, some representative mesh points can also be selected as design variables.

In the present study, vertical (y) coordinates of all of the surface meshes are employed as design variables for both two- and three-dimensional design examples.

B. Volume Mesh Modification

When the surface meshes are modified by a design update, the interior volume meshes should also be modified accordingly. In the two-dimensional cases with structured meshes, the interior mesh positions are moved with relative ease using a mesh movement strategy that modifies mesh coordinates along a mesh line of the same index of the generalized coordinate ξ in an algebraic manner.

In the three-dimensional examples with unstructured meshes, we use a robust mesh-point movement method utilizing a spring analogy based on a torsion spring concept.[16]

C. Design Procedure

In the present study, the steepest descent method is adopted for the gradient-based optimization:

$$X^{\mathrm{new}} = X^{\mathrm{old}} - \lambda \nabla F \tag{20}$$

Instead of objective function gradient $-\nabla F$, we use the smoothed deformation ΔX obtained by the traction method:

$$X^{\mathrm{new}} = X^{\mathrm{old}} + \lambda \Delta X \tag{21}$$

where λ is selected by a line search method. For the line search along the smoothed deformation vector, linear or quadratic methods are adopted. Firstly, the linear line search method is used to obtain an objective function smaller than the one of the preceding design iteration. If the objective function is improved from the preceding one by the linear line search, we go on to the next design iteration. If this is not the case, a quadratic line search is conducted, which requires an additional flow analysis along the search direction. An allowable range of the surface modification can also be imposed during the line search process. The design process is terminated when the design shows no improvement for three consecutive design iterations.

By comparing Eqs. (20) and (21), one can note that the geometric deformation vector ΔX is regarded as a negative of the smoothed gradient. As mentioned in the Introduction, gradient smoothing is expected to act as a preconditioner to reduce the number of design iterations needed for convergence.[1]

Figure 5 shows the design procedure using the present design method. For given flow conditions, objective function, constraints, and mesh for the initial geometry, the flowfield is analyzed by a flow solver. With the converged solution of flow variables, an adjoint

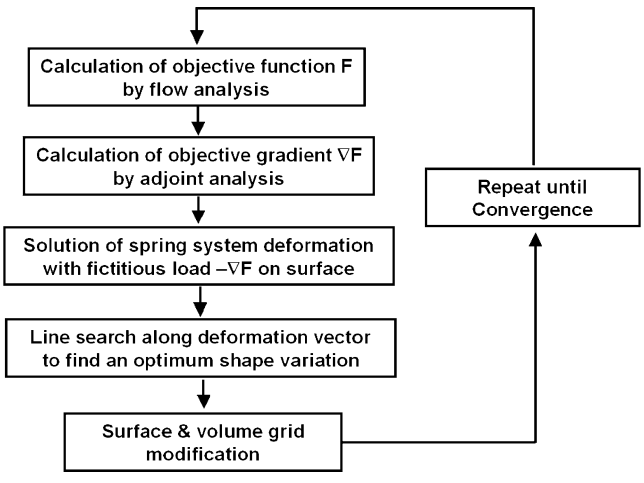

Fig. 5 Design procedure.

analysis is conducted for sensitivity analysis. Then the sensitivity gradient vector is imposed on the spring system of surface mesh points as fictitious external forces. The deformation vector is considered as a smoothed gradient vector and used for the line search process. An optimum shape variation obtained by a linear or quadratic line search process is added to the preceding geometry, and volume mesh is modified according to the surface mesh modification. This procedure is repeated until convergence.

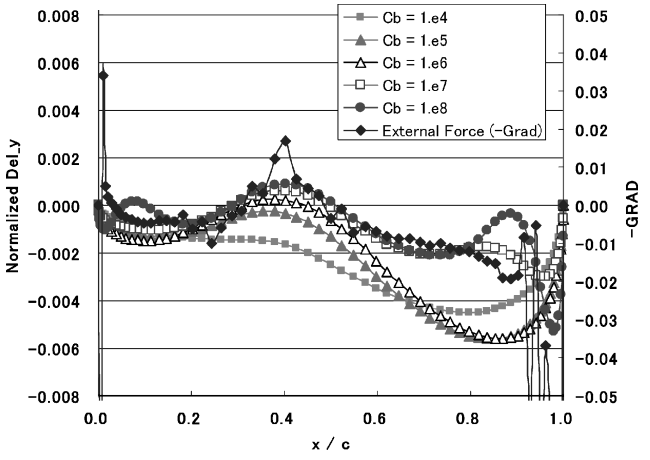

a) Lower surface

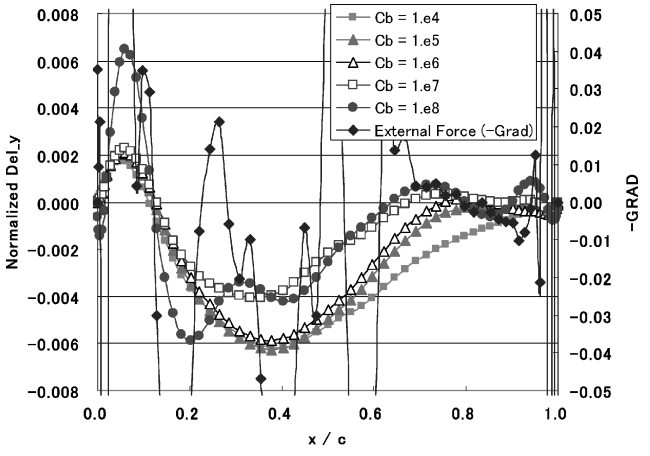

b) Upper surface

Fig. 6 Gradient and deformation for the first iteration of inverse design with various bending constants.

V. Design Examples

For the validation of the present approach using the traction method and the spring analogy, design problems of two-dimensional airfoils and three-dimensional aircraft configurations are conducted.

A. Two-Dimensional Design Examples

1. Inverse Design

Design conditions are a freestream Mach number of 0.73, an incidence angle α of 2.7 deg, and a Reynolds number of 7×10^6. The design objective function is defined as follows:

Minimize:

$$F = \frac{1}{2}\sum_{i=1}^{N_{\text{node}}}(P_c - P_t)_i^2 \Delta x_i$$

where p_c and p_t are computed and target pressures, respectively. The initial airfoil is RAE2822, and the target airfoil is NACA0012. The flow solver is run in a fixed α mode, and leading-edge and trailing-edge nodes are kept fixed throughout the design procedure. Because the initial and target airfoils have different trailing-edge angles, the bending spring constant of the trailing-edge node is set to zero so that the bending spring force on the trailing-edge mesh does not hamper design convergence to the target airfoil shape.

Figure 6 shows the objective function gradient calculated by the adjoint code and the geometry deformation (or "smoothed" gradient) obtained by the traction method for the first iteration of the inverse design with various bending constants C_b.The resulting deformations are scaled appropriately for purposes of comparison. The initial gradient oscillates especially near the leading and trailing edges. The geometric deformation is closest to the external forces when the bending constant C_b has the largest value, and the geometry deformation becomes smoother as the bending constant C_b decreases. This is because the effect of the tension spring forces becomes dominant as the C_b decreases because the magnitude of bending spring forces decreases. The balance between closeness to the actual gradient and smoothness of the design geometry can be controlled by adjusting C_b.

The bending constant C_b can be selected empirically or by trial and error. For trial and error, the resulting geometric variation for the first design iteration can be investigated for various bending constants as is done in this study because the magnitude of geometry deformation for the first design iteration is usually the largest of the design iterations. In addition, data files of converged solutions of the flow solver and the adjoint code for the initial geometry are ready for the code restart at the first design iteration, and thus the computational burden of the test of several bending constants is negligible. A recommendation on selection of the bending constant is made in Sec. V.C.

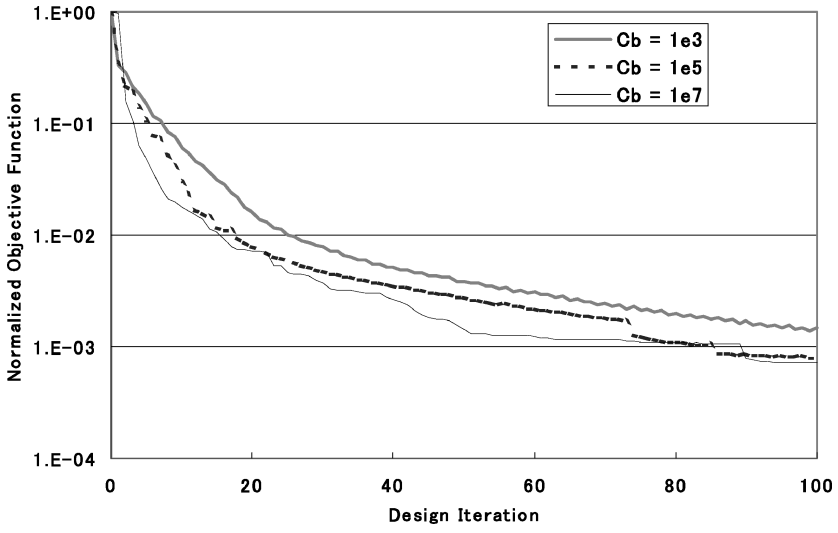

Fig. 7 Convergence history of two-dimensional inverse design for various bending constants.

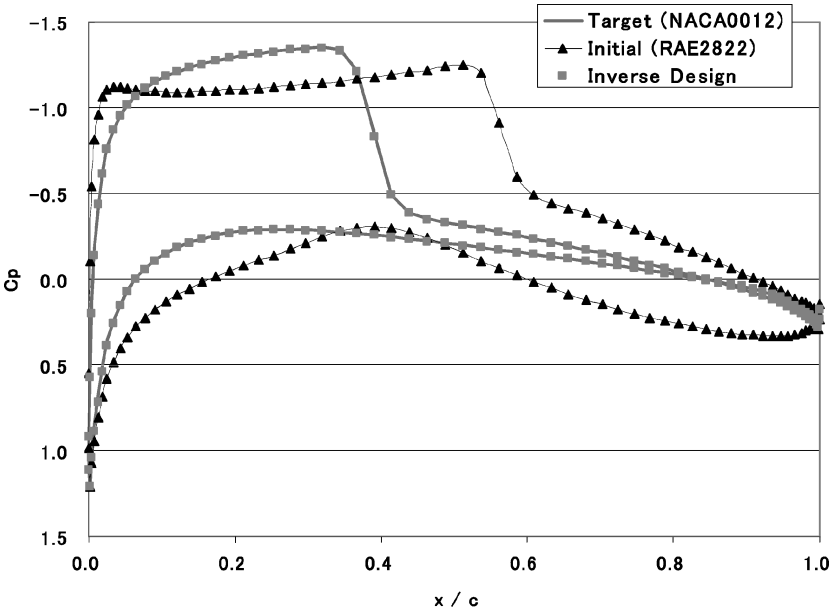

a) Surface-pressure distributions

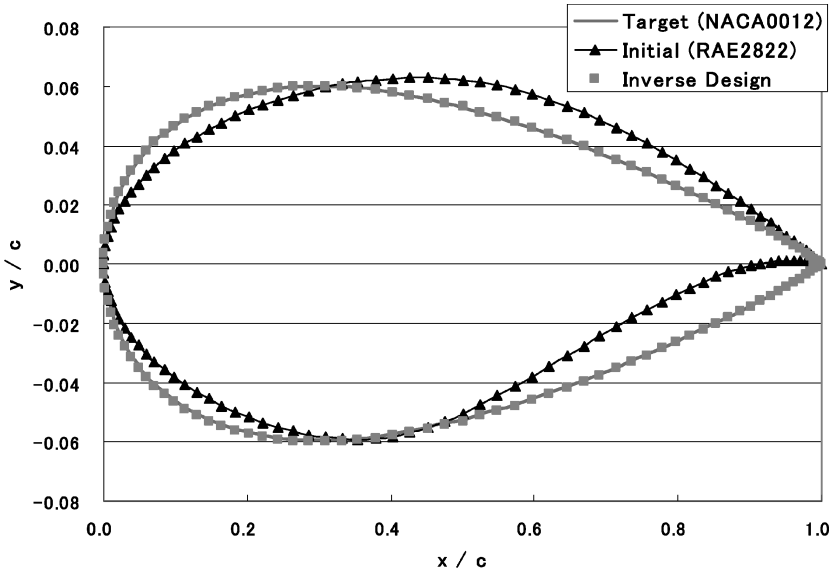

b) Airfoil shapes

Fig. 8 Results of two-dimensional inverse design.

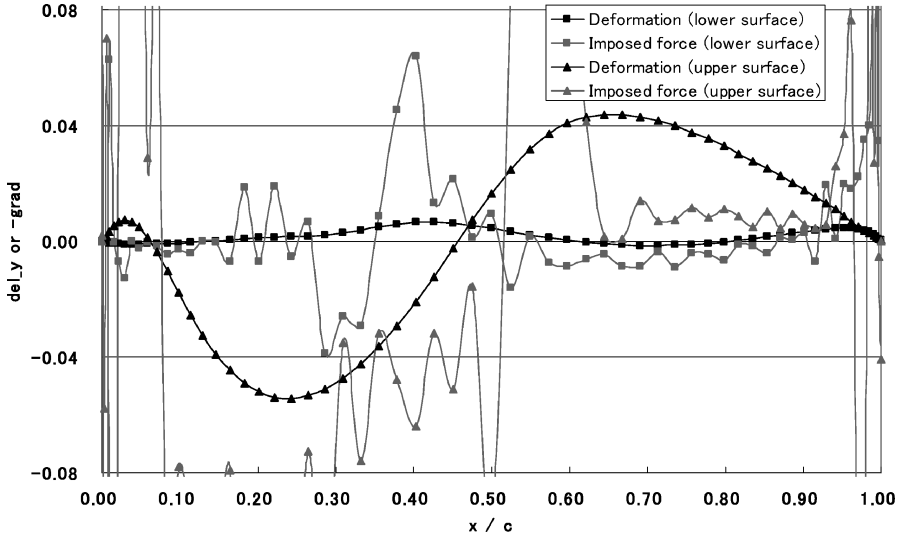

Fig. 9 Gradient and deformation for the first iteration of two-dimensional direct design ($C_b = 10^4$).

Design histories of inverse designs with various bending constants are shown in Fig. 7. A larger bending constant gives a better design convergence. This is consistent with the results in Fig. 6 that larger bending constant yields a deformation closer to the actual gradient obtained by the adjoint code, although some other factors also affect the design convergence.

The final result of the inverse design is presented in Fig. 8. The design airfoil shape and pressure distribution coincide with the target airfoil almost exactly.

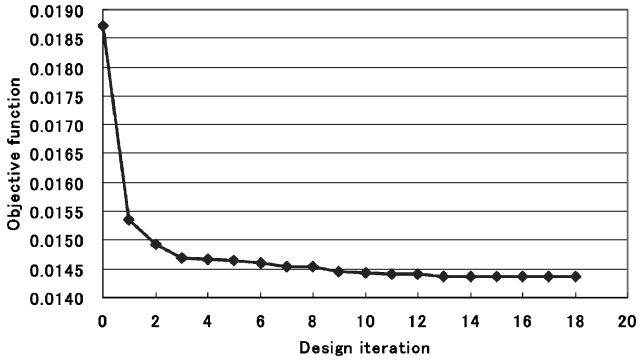

Fig. 10 Convergence history of two-dimensional direct design.

2. Direct Design

The objective of the direct design example is defined as follows:

$$\text{Minimize} \quad C_d$$

$$\text{Subject to} \quad C_l \geq C_l^*$$

$$\text{Area} \geq \text{area}^*$$

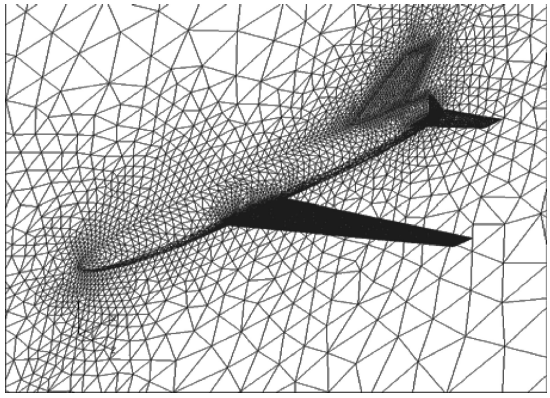

Fig. 12 Initial surface meshes on ONERA M5.

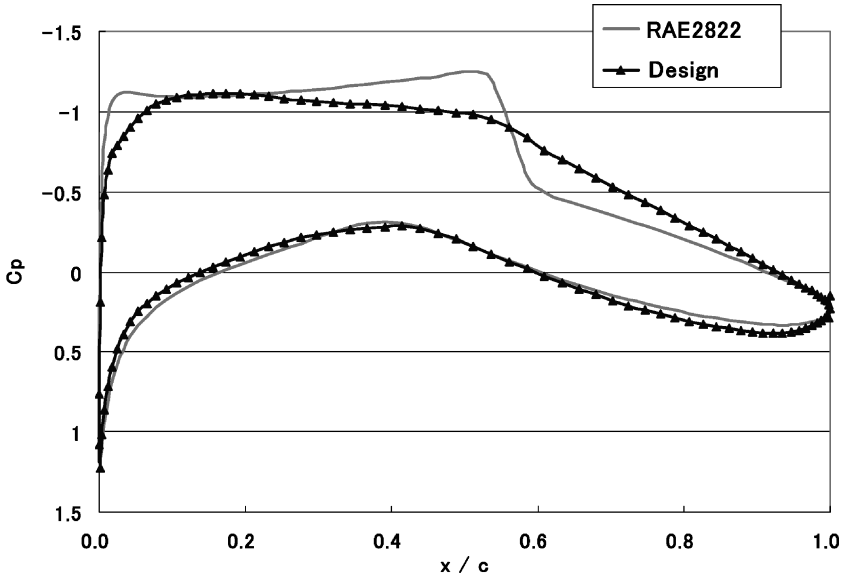

a) Surface-pressure distribution

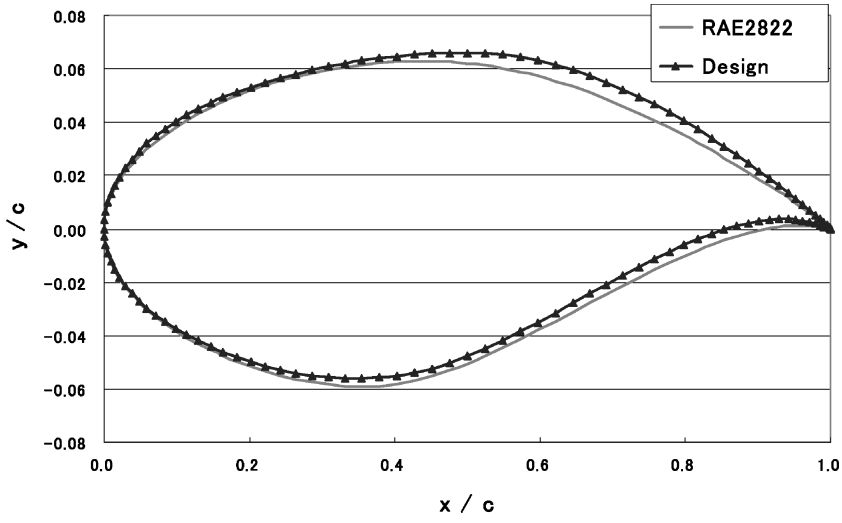

b) Airfoil shape

Fig. 11 Results of two-dimensional direct design.

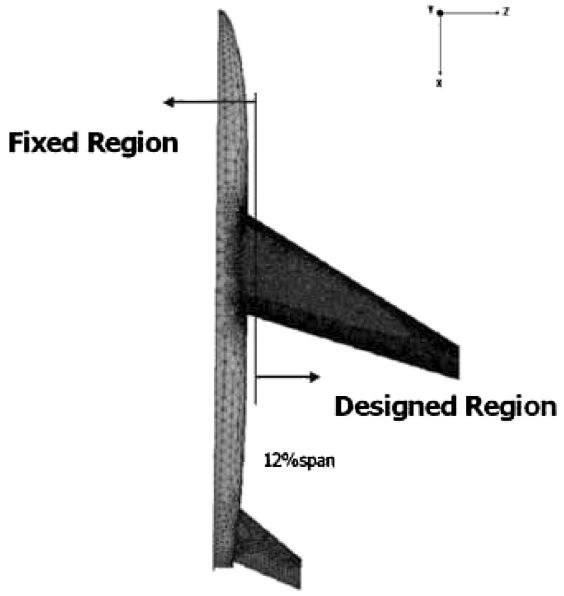

Fig. 13 Design region in ONERA M5 wing design.

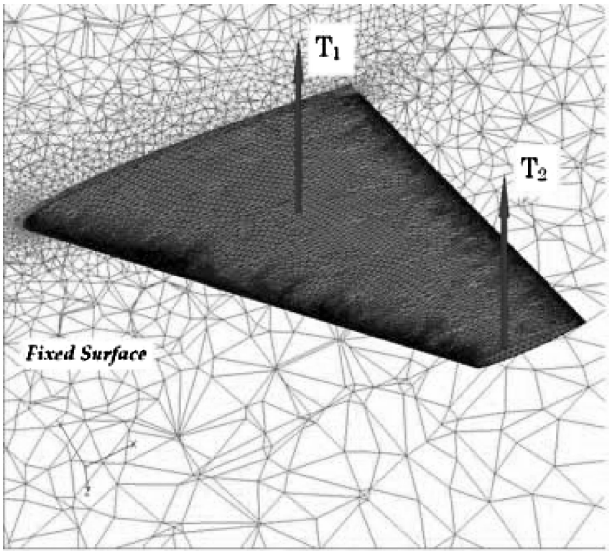

a) Applied singular forces

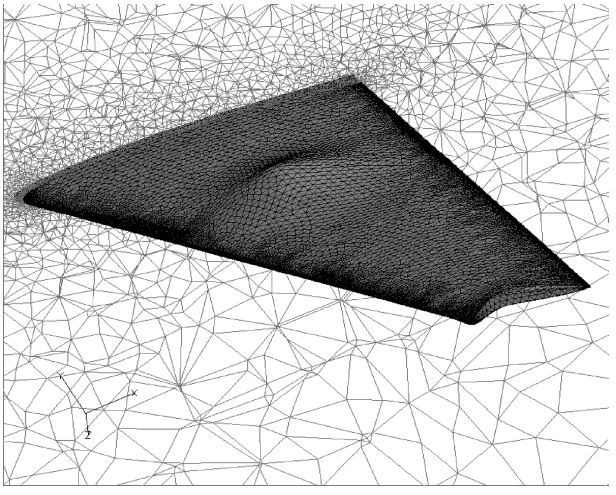

b) Deformed mesh

Fig. 14 ONERA M5 wing surface deformation by singular forces using traction method.

where C_d and C_l are drag and lift coefficients of an airfoil and C_l^* is a target lift coefficient, which is the same as the initial lift coefficient. Area is the airfoil section area.

If the lift constraint is dealt with as an explicit constraint in the design optimization procedure, it requires an additional adjoint analysis for the C_l gradient calculation per design iteration. In this study, therefore, the lift constraint is satisfied by running the flow solver in the fixed-lift mode, in which the incidence angle α is adjusted based on $C_{l\alpha}$.

Because we would like to minimize drag when $C_l = C_l^*$, that is, at an adjusted incidence angle, the objective function $F = C_d$ should be modified as follows to consider the lift constraint consistently:

$$F = C_d^* = C_d + \frac{\partial C_d}{\partial \alpha}\Delta\alpha \tag{22}$$

where C_d is a drag coefficient without any incidence angle modification and $\Delta\alpha$ is a required incidence angle variation to match the lift with the target lift. A similar relation can be written for the lift coefficient:

$$C_l^* = C_l + \frac{\partial C_l}{\partial \alpha}\Delta\alpha \tag{23}$$

where C_l is a lift coefficient without any incidence angle variation and C_l^* is the target lift coefficient. If we arrange the preceding equation for $\Delta\alpha$ and input it into Eq. (22), we obtain a modified objective function as follows[6,7]:

$$F = C_d - (Cd_\alpha/Cl_\alpha)\left(C_l - C_l^*\right) \tag{24}$$

where the second term in the right-hand side with lift coefficients acts as a penalty term preventing the design from reducing the drag by simply reducing the lift.

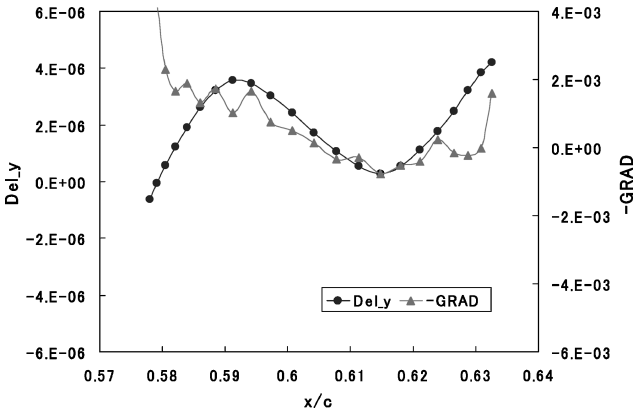

a) Lower surface

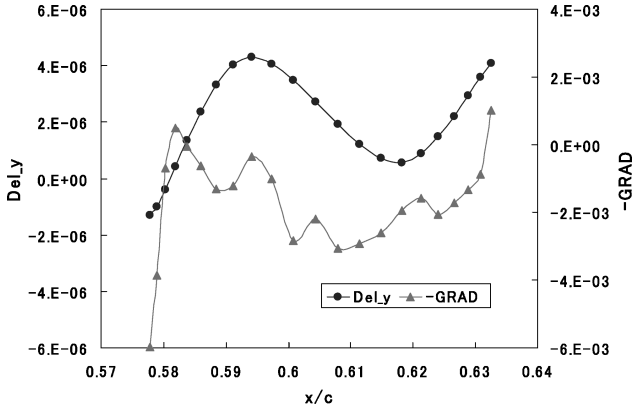

b) Upper surface

Fig. 15 Gradient and deformation at ONERA M5 wing-tip surface ($C_b = 10^8$).

Similarly, we define C_{dA} as an additional drag variation by the area change to match the target area. We make an assumption that the drag variation is propotional to the area change, that is,

$$C_{\mathrm{dA}} \cong -C_d \frac{(\text{area} - \text{area}^*)}{\text{area}} \cong -C_{d0} \frac{(\text{area} - \text{area}^*)}{\text{area}} \tag{25}$$

where C_{d0} is the drag coefficient of the initial airfoil. Note that C_{dA} is only a function of geometric variables. The gradient vector of C_{dA} is added to the objective function gradient calculated by the adjoint method to obtain a modified gradient of objective function for the area constraint. This acts to project the original gradient vector into the feasible design space[27]:

$$\nabla F_m = \nabla F + w \nabla C_{\mathrm{dA}} \tag{26}$$

where w is a parameter ranging from 0.5 to 1.5 to adjust the magnitude of the area penalty term. The modified gradient of Eq. (26) is used for external forces in the design process of the present study.

Figure 9 shows the gradient and shape deformation at the first design iteration of the present direct design. The shape deformation is magnified to permit easy comparison. The gradient vector is discontinuous and severely oscillates, especially near the leading and trailing edges. On the other hand, the shape deformation is very smooth while following the overall trend of the gradient vector.

Figure 10 shows the convergence history of the direct design with the bending constant C_b of 10^4. The airfoil shapes and pressure distributions are presented in Fig. 11. A shock-free airfoil is obtained by 18 design iterations. The aerodynamic coefficeints of the design airfoils are shown in Table 1. The drag is remarkably reduced while satisfying the imposed constraints on the lift and airfoil section area.

B. Three-Dimensional Design Examples

For the validation of the present design approach in three-dimensional design optimization problems, design examples of an ONERA M5 wing and a supersonic transport (SST) fuselage shape

Table 1 Results of two-dimensional direct design

Aerodynamic performance	*CL*	*CD*	L/D[a]	Area
Initial (RAE2822)	0.7386	0.01873	41.84	0.07784
Design	0.7844	0.01452	54.01	0.07841
Δ, %	+6.2	−22.5	+29.1	+0.7

[a] L/D = lift-to-diag ratio.

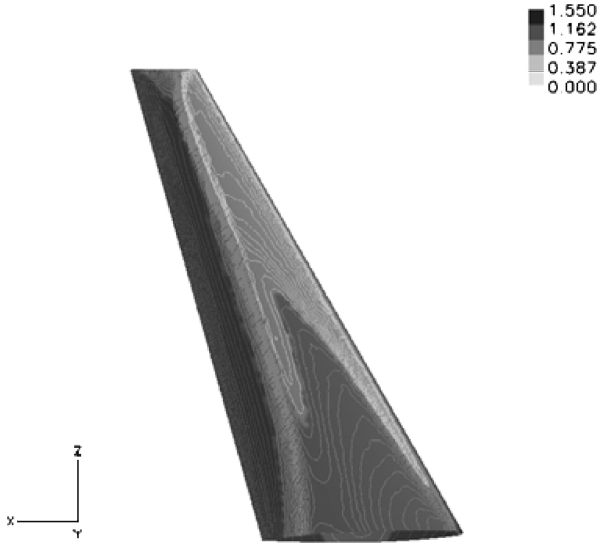

a) Initial

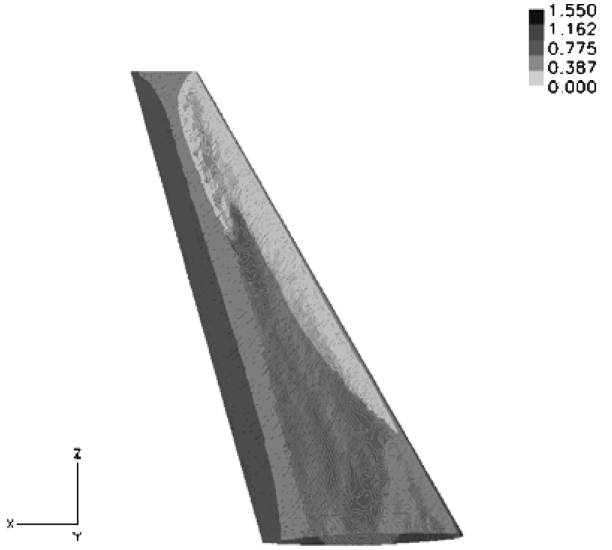

b) Design

Fig. 17 Comparison of ONERA M5 wing upper-surface-pressure contours of ONERA M5.

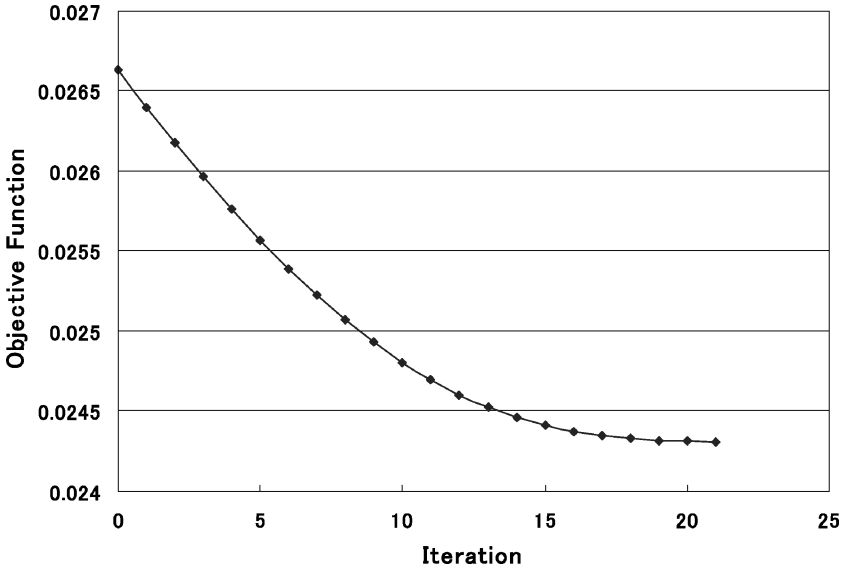

Fig. 16 Convergence history of ONERA M5 design.

were performed. All of the computations were conducted on an NEC SX-7 vector computer of Tohoku University Synergy Center. The coordinate system was employed as follows: x for the streamwise direction, y for the upward direction, and z for the spanwise direction.

1. Optimization of the ONERA M5 Wing

The present design method is applied to the ONERA M5 main wing design. The surface mesh points are generated by a direct advancing front method coupled with geometrical feature extraction on the stereolithography (STL) data format.[28] A tetrahedral volume mesh is generated by a Delaunay-type generation method.[29] Figure 12 shows the surface mesh of the ONERA M5 configuration containing 113,132 mesh points and 606,110 tetrahedrons. As for design variables, wing surface mesh points of $z \geq 0.06$ are employed as shown in Fig. 13. All other surface mesh points with $z < 0.06$ are kept fixed as in the clamp condition in a cantilever beam problem. The total number of design variables is 14,107.

Before conducting design optimization, two singular fictitious loads ($T_1 = T_2 = 1.0$) are imposed on the ONERA M5 wing surface as shown in Fig. 14a for a simple validation of the present traction method. The deformed shape is shown in Fig. 14b in which the geometric variations are magnified by 500 times. Even though the singular forces are applied to the surface mesh points, smooth geometric variations are obtained by the present traction method approach.

As a design example, the design method is applied to an ONERA M5 main wing. Design conditions are a freestream Mach number of

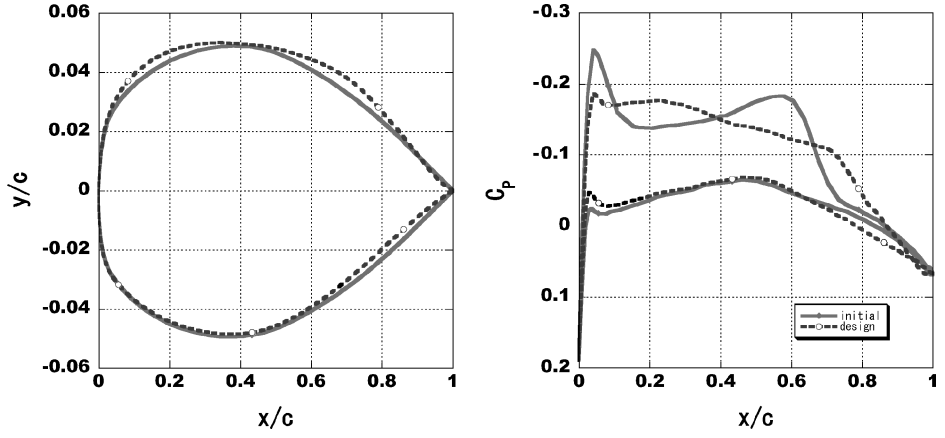

a) $z = 0.14$ (28.5% span)

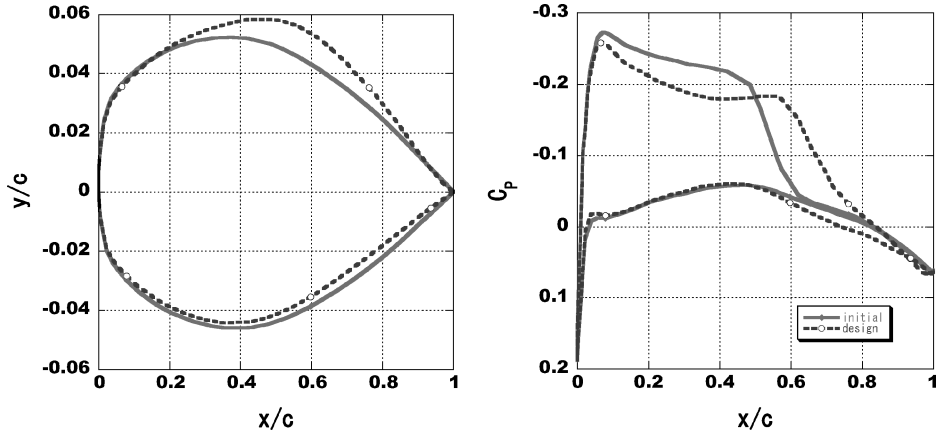

b) $z = 0.30$ (61.1% span)

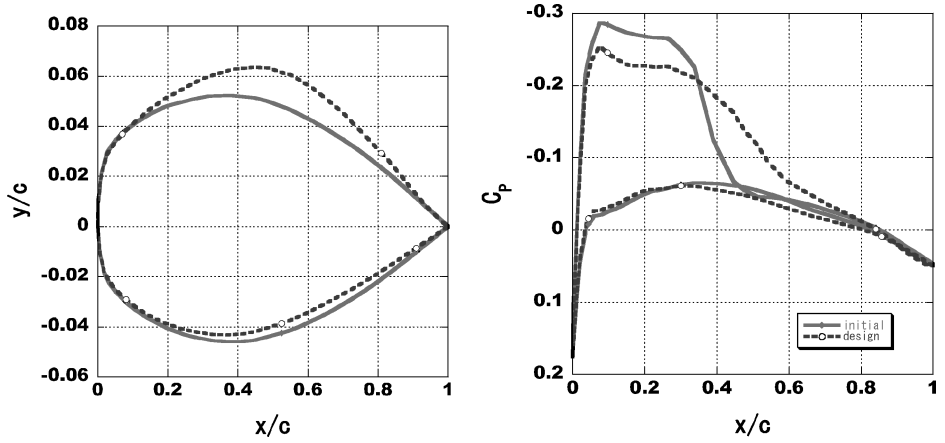

c) $z = 0.43$ (87.6% span)

Fig. 18 Wing-section shapes and surface-pressure distributions for ONERA M5 design.

0.84 and C_L of 0.256 with an initial angle of attack $\alpha = -1.0$ deg. The objective of this design study is defined as follows:

$$\begin{aligned} &\text{Minimize} && C_D \\ &\text{Subject to} && C_L \geq C_L^* \\ & && V \geq V^* \end{aligned} \tag{27}$$

where V represents the wing volume and * represents a target value, which is an initial value in this case.

The lift constraint is satisfied by running the flow solver in the fixed-lift mode, in which the incidence angle is adjusted periodically during flow analysis based on $C_{L\alpha}$ and the objective function is modified as in the two-dimensional case in Eq. (24). The volume constraint is also treated by the gradient projection, which was adopted for two-dimensional area constraints.

Figure 15 shows the initial gradient calculated by the adjoint code and geometry deformation (or smoothed gradient) obtained by the traction method for the first iteration of the design with the bending constant C_b of 10^8. Although the gradient vector oscillates, the deformation is smooth and follows the trend of the gradient vector. However, some deviations can occur because all of the objective gradients on the surface meshes other than those on the tip section also affect the wing-tip deformation.

Table 2 presents the design results after 21 design iterations. The drag coefficient is reduced by 23 counts while satisfying the lift and volume constraints. Figure 16 shows the convergence history of the design with the bending constant C_b of 10^8. Strength of the λ shock wave is remarkably reduced by the design as shown in Fig. 17. Wing-section shapes and pressure distributions at several wing sections are compared in Fig. 18. Section pressure distributions also show that the strength of the shock wave has been remarkably reduced.

2. Fuselage Shape Optimization of SST Airplane with Nacelles

In the second design example, the present design tool is applied to the fuselage shape of the SST airplane NEXST-2 (National experimental Supersonic Transport). This experimental airplane was designed to cruise at a speed of Mach 2.0 by the National Aerospace Laboratory of Japan using aerodynamic design technology together with CFD prediction.[30] The SST configuration and its surface mesh are shown in Fig. 19. The computational grid contains 848,772 mesh points and 4,781,123 tetrahedrons. All of the fuselage surface mesh points are allowed to move in the vertical direction, and the mesh points on fuselage-wing junction and fuselage-tail junction lines are kept fixed. Consequently, 6061 surface meshes are used as design variables.

Design conditions are a freestream Mach number of 1.7 and C_L of 0.0668 with an initial angle of attack $\alpha = 0$ deg. Although the design objective is same as Eq. (27), the fuselage volume instead of the wing volume is constrained.

After deformation of the fuselage shape, grid points on the symmetry boundary surface also need to be moved accordingly. This two-dimensional unstructured grid modification was also performed by the dynamic mesh-point movement method suggested by Murayama et al.[16] This design example is performed with the bending constant C_b of 10^8.

After five design iterations, the drag coefficient is reduced by three drag counts while satisfying the lift and fuselage volume constraints as shown in Table 3. Drag reduction in this example is not so remarkable because the initial geometry is already in its optimized configuration. The amount of the drag reduction is similar

a) Configuration

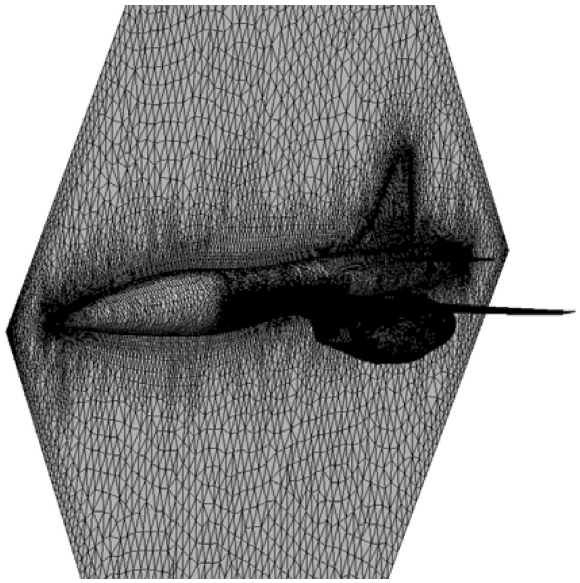

b) Surface mesh

Fig. 19 Configuration and surface mesh of NEXST-2.

Table 2 Results of ONERA M5 wing design

Aerodynamic performance	C_L	C_D	L/D	Wing volume
Initial	0.2560	0.02664	9.61	5.00×10^{-4}
Design	0.2560	0.02431	10.53	5.08×10^{-4}
Δ, %	+0.0	−8.75	+9.57	+1.60

Table 3 Results of NEXST-2 fuselage design

Aerodynamic performance	C_L	C_D	L/D	Fuselage volume
Initial	0.0668	0.01888	3.54	6.182×10^{-4}
Design	0.0668	0.01858	3.60	6.191×10^{-4}
Δ, %	+0.0	−1.59	+1.69	+0.16

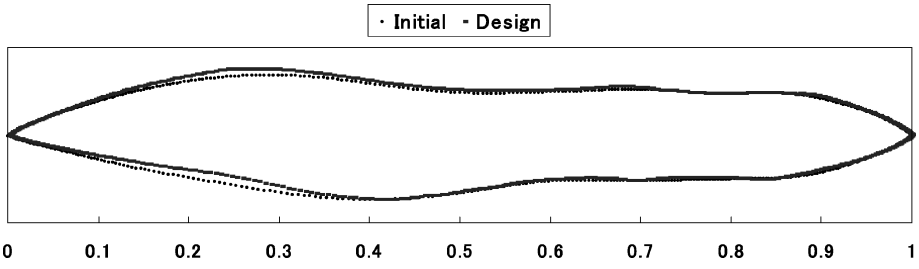

Fig. 20 Initial and design configurations of NEXST-2 (side view).

Table 4 Bending constant values used in the design examples

	Two dimensions		Three dimensions	
Design example	Inverse	Direct	ONERA M5 wing	NEXST-2 fuselage
Averaged edge length	$\mathcal{O}(10^{-2})$	$\mathcal{O}(10^{-2})$	$\mathcal{O}(10^{-3})$	$\mathcal{O}(10^{-2})$
Bending constant C_b	10^7	10^4	10^8	10^8

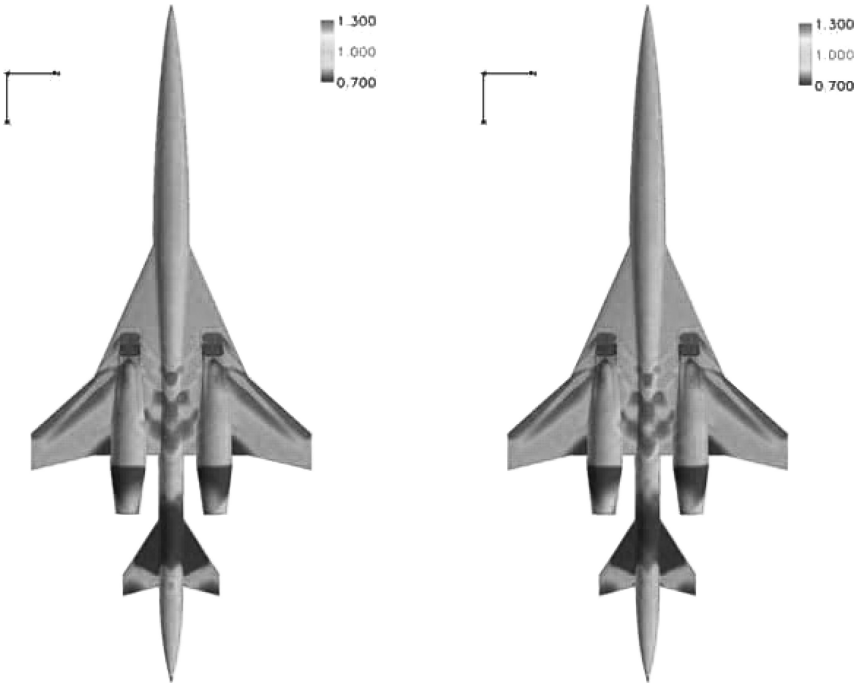

a) Initial **b) Design**

Fig. 21 Pressure contours on the lower surface of NEXST-2.

to the results of Ref. 31 on the optimization of NEXST-2 fuselage shape.

Figure 20 compares the initial and final design configurations of the NEXST-2 fuselage geometry. Comparison of the surface-pressure contours on the lower surface of the airplane in Fig. 21 shows a slight difference in surface pressures. It should be noted from the C_P distributions of a wing section near the root in Fig. 22 that the optimized shape reduced the strength of the shock wave on the lower wing surface.

Although the wing or fuselage shapes are designed as examples of three-dimensional design, configurations with discontinuous curvatures such as wing-fuselage junctions can also be treated with the present method as in the case of Sobolev implicit smoothing applied to designs of entire aircraft in Refs. 1 and 9.

C. Discussion on Selection of Bending Constant C_b

In the present surface modification method combining the traction method and spring analogy, the bending constant C_b needs to be selected so as to control the balance of the geometric deformation vector between closeness to the actual gradient and smoothness of geometric variation. As mentioned in Sec.V.A.1, the geometric deformation becomes smoother (or flatter) as the bending constant C_b decreases. This is because the effect of the tension spring forces becomes dominant as C_b decreases. And as C_b increases, the deformation becomes wavier.

The values of C_b used in the design examples in two and three dimensions are presented in Table 4. During the design studies, it was found that the objective gradients for three-dimensional cases oscillate much less than two-dimensional cases. Thus, larger values of C_b can be used for three-dimensional cases than for two-dimensional cases.

By its nature, the inverse design also results in a more stable design process than the direct design. For these reasons, a smaller value of

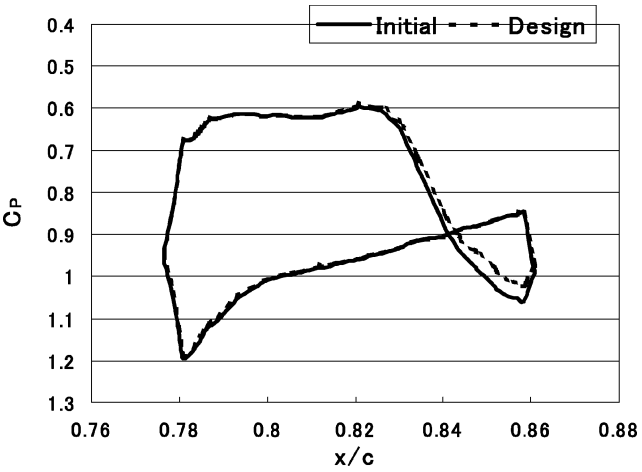

Fig. 22 Surface-pressure distributions at a wing section of 14.6% span of NEXST-2.

C_b should be used in the two-dimensional direct design case than in the two-dimensional inverse case. Overall, C_b lower than those in Table 4 would result in smoother and more stable geometric variations.

The selection of bending constant depends on the smoothness of the objective function gradient, as well as on grid density and definition of the design objective, etc., all of which vary for specific design problems.

For example, the values recommended in Table 4 might need to be altered if the surface mesh density is changed drastically. If a coarser mesh is used, the tension stiffness is reduced, which causes more oscillating (or wavy) deformation while other conditions remain the

same. This means a smaller C_b might need to be used to prevent a wavy design surface, and vice versa for a finer mesh. However, the dependency on the grid density is only on the order of the edge lengths and is not so critical.

VI. Conclusions

For the mesh-point approach using all of the surface mesh points as design variable, a new method for geometric modification in aerodynamic design optimization has been developed combining the traction method and spring analogy. The design surface mesh is represented as a spring system with tension and bending springs located at edges and nodes of the surface mesh. The negative gradient of the objective function is imposed on the surface nodes as fictitious external forces. The resultant deformation is considered as a smoothed direction vector, and a line search is conducted along the direction vector. The method resulted in smooth variation of design surfaces even for singular fictitious forces while Sobolev implicit smoothing yielded a peaky variation.

For the validation of the present method, two- and three-dimensional design examples were conducted. Successful results of the design examples validate that the present method allows smooth and robust modification of aerodynamic design surfaces. A recommendation on selection of the value of the parametric bending constant was made based on results of the present numerical study.

References

[1]Jameson, A., "Aerodynamic Shape Optimization Using the Adjoint Method," Lecture Series, Vol. 2, Von Kármán Inst. for Fluid Dynamics, Brussels, Feb. 2003.

[2]Kim, S., Alonso, J. J., and Jameson, A., "Design Optimization of High-Lift Configurations Using a Viscous Continuous Adjoint Method," AIAA Paper 2002-0844, Jan. 2002.

[3]Kim, C. S., Kim, C., and Rho, O. H., "Sensitivity Analysis for the Navier–Stokes Equations with Two-Equation Turbulence Models," *AIAA Journal*, Vol. 39, No. 5, 2001, pp. 838–845.

[4]Nielson, E. J., and Anderson, W. K., "Aerodynamic Design Optimization on Unstructured Meshes Using the Navier–Stokes Equations," *AIAA Journal*, Vol. 37, No. 11, 1999, pp. 1411–1419.

[5]Anderson, W. K., and Bonhaus, D. L., "Airfoil Design on Unstructured Grids for Turbulent Flows," *AIAA Journal*, Vol. 37, No. 2, 1999, pp. 185–191.

[6]Reuther, J. J., Jameson, A., Alonso, J. J., Rimlinger, M. J., and Saunders, D., "Constrained Multipoint Aerodynamic Shape Optimization Using an Adjoint Formulation and Parallel Computers, Part 1," *Journal of Aircraft*, Vol. 36, No. 1, 1999, pp. 51–60.

[7]Kim, H. J., Sasaki, D., Obayashi, S., and Nakahashi, K., "Aerodynamic Optimization of Supersonic Transport Wing Using Unstructured Adjoint Method," *AIAA Journal*, Vol. 39, No. 6, 2001, pp. 1011–1020.

[8]Kim, H. J., Kim, C., Rho, O. H., and Lee, K., "Aerodynamic Sensitivity Analysis for Navier–Stokes Equations," AIAA Paper 99-0402, Jan. 1999.

[9]Mohammadi, B., "Optimal Shape Design, Reverse Mode of Automatic Differentiation and Turbulence," AIAA Paper 97-0099, Jan. 1997.

[10]Samareh, J., "Survey of Shape Parameterization Techniques for High-Fidelity Multidisciplinary Shape Optimization," *AIAA Journal*, Vol. 39, No. 5, 2001, pp. 877–884.

[11]Wu, H.-Y., Yang, S., Liu, F., and Tsai, H.-M., "Comparison of Three-Geometric Representations of Airfoils for Aerodynamic Optimization," AIAA Paper 2003-4095, June 2003.

[12]Azegami, H., "A Solution to Domain Optimization Problems," *Transactions of the Japan Society of Mechanical Engineers (A)*, Vol. 60, No. 574, 1994, pp. 1479–1486 (in Japanese).

[13]Azegami, H., and Wu, Z., "Domain Optimization Analysis in Linear Elastic Problems: Approach Using Traction Method," *JSME International Journal, Series A*, Vol. 39, No. 2, 1996, pp. 272–278.

[14]Katamine, E., and Azegami, H., "Domain Optimization Analysis of Potential Fluid Flow (Approach by the Traction Method)," *Transactions of the Japan Society of Mechanical Engineers (B)*, Vol. 61, 1995, pp. 103–108 (in Japanese).

[15]Belegundu, A. D., and Rajan, S. D., "A Shape Optimization Approach Based on Natural Design Variables and Shape Functions," *Computer Methods in Applied Mechanics and Engineering*, Vol. 66, No. 1, 1988, pp. 87–106.

[16]Murayama, M., Nakahashi, K., and Matsushima, K., "Unstructured Dynamic Mesh for Large Movement and Deformation," AIAA Paper 2002-0122, Jan. 2002.

[17]Blom, F. J., "Considerations on the Spring Analogy," *International Journal for Numerical Methods in Fluids*, Vol. 32, No. 6, 2000, pp. 647–668.

[18]Hwang, S. W., "Numerical Analysis of Unsteady Supersonic Flow over Double Cavity," Ph. D. Dissertation, Dept. of Aerospace Engineering, Seoul National Univ., Seoul, Republic of Korea, Feb. 1996.

[19]Kim, H. J., and Rho, O. H., "Dual-Point Design of Transonic Airfoils Using the Hybrid Inverse Optimization Method," *Journal of Aircraft*, Vol. 34, No. 5, 1997, pp. 612–618.

[20]Roe, P. L., "Approximate Riemann Solvers, Parameter Vectors, and Difference Schemes," *Journal of Computational Physics*, Vol. 43, No. 2, 1981, pp. 357–372.

[21]Van Leer, B., "Toward the Ultimate Conservative Difference Scheme., A New Approach to Numerical Convection," *Journal of Computational Physics*, Vol. 23, No. 3, 1977, pp. 276–299.

[22]Baldwin, B. S., and Lomax, H.,"Thin-Layer Approximation and Algebraic Model for Separated Turbulent Flow," AIAA Paper 78-0257, Jan. 1978.

[23]Venkatakrishnan, V., "On the Accuracy of Limiters and Convergence to Steady State Solutions," AIAA Paper 93-0880, Jan. 1993.

[24]Obayashi, S., and Guruswamy, G. P., "Convergence Acceleration of an Aeroelastic Navier–Stokes Solver," *AIAA Journal*, Vol. 33, No. 6, 1995, pp. 1134–1141.

[25]Sharov, D., and Nakahashi, K., "Reordering of Hybrid Unstructured Grids for Lower-Upper Symmetric Gauss-Seidel Computations," *AIAA Journal*, Vol. 36, No. 3, 1998, pp. 484–486.

[26]Ahn, J., Kim, H. J., Lee, D. H., and Rho, O. H., "Response Surface Method for Airfoil Design in Transonic Flow," *Journal of Aircraft*, Vol. 38, No. 2, 2001, pp. 231–238.

[27]Vanderplaats, G. N., *Numerical Optimization Techniques for Engineering Design: With Applications*, McGraw–Hill, New York, 1984, pp. 163–166.

[28]Ito, Y., and Nakahashi, K., "Direct Surface Triangulation Using Stereolithography Data," *AIAA Journal*, Vol. 40, No. 3, 2002, pp. 490–496.

[29]Sharov, D., and Nakahashi, K., "A Boundary Recovery Algorithm for Delaunay Tetrahedral Meshing," *5th International Conference on Numerical Grid Generation in Computational Field Simulations*, edited by B. K. Soni, J. F. Thompson, J. Häuser, and P. R. Eiseman, Mississippi State Univ., Mississippi State, MS, 1996, pp. 229–238.

[30]Iwamiya, T., "NAL SST Project and Aerodynamic Design of Experimental Aircraft," *Proceedings of the Computational Fluid Dynamics'98, ECCOMAS 98*, Vol. 2, Wiley, New York, 1998, pp. 580–585.

[31]Makino, Y., Iwamiya, T., and Lei, Z., "Fuselage Shape Optimization of a Wing-Body Configuration with Nacelles," *Journal of Aircraft*, Vol. 40, No. 2, 2003, pp. 297–302.

M. Ahmadian
Associate Editor